

Microscopic investigation of wobbling motion in atomic nuclei using the triaxial projected shell model approach

J.A. Sheikh^{1,2}, S. Jehangir² and G. H. Bhat³

¹ *Department of Physics, University of Kashmir, Srinagar, 190 006, India*

² *Department of Physics, Islamic University of Science and Technology, Kashmir, India*

³ *Department of Physics, Govt. Degree College, Shopian, India*

Abstract

A systematic investigation of the wobbling band structures observed in odd-mass nuclei of $^{161,163,165,167}\text{Lu}$, ^{167}Ta , ^{131}Cs , ^{135}Pr , ^{151}Eu , ^{183}Au , ^{133}Ba , ^{105}Pd , ^{133}La , ^{187}Au and ^{127}Xe is performed using the triaxial projected shell model (TPSM) approach. It is demonstrated that all the studied band structures have transverse wobbling mode, except for ^{133}La , ^{187}Au (negative parity), ^{183}Au (positive parity) and ^{127}Xe nuclei where the wobbling frequency increases with spin, indicating that the collective motion has a longitudinal character. To elucidate further the wobbling nature of the band structures, electromagnetic transition probabilities have been evaluated and it is observed that inter-band transitions are dominated by $E2$ rather than $M1$ as expected for a typical signature partner band. It is shown that TPSM approach provides a reasonable description of all the measured properties of the studied nuclei.

1 Introduction

Atomic nuclei depict a rich diversity of shapes and structures, primarily driven by the quantum mechanical shell effects and to elucidate these features microscopically is one of main research themes in nuclear physics [1]. The information regarding the nuclear shape is inferred through a comparison of the measured quantities with the predictions of a theoretical model that assumes a geometrical shape for the atomic nucleus in the intrinsic frame of reference. The unified model of Bohr and Mottelson has played a key role in our understanding of nuclear shapes [2]. In this model, the shape is assumed to have dominant quadrupole degree of freedom and is parametrized in terms of axial and non-axial deformation parameters of β and γ . Most of the deformed nuclei have prolate shapes with $\gamma = 0^\circ$, and there are also some nuclei with oblate spheroidal shape having $\gamma = 60^\circ$. These nuclei are referred to as axial and have the projection of the angular momentum along the symmetry

axis, designated by “K”, a conserved quantum number. There are selection rules based on this conserved quantity, for instance, Alaga rules and nuclei in many regions of the periodic table are known to follow the selection rules based on the K-quantum number [2].

Nevertheless, there are also a few regions in nuclear chart for which axial symmetry is predicted to be broken with $0 < \gamma^\circ < 60$. The regions include $A \sim 160$ [3,4,5,6,7,8,9,10] and $A \sim 130$ [11,12,13,14,15]. These nuclei, referred to as triaxial systems, have unequal moments of inertia along the three principle axes (short axis s , medium axis m and long axis l) and the rotational motion can lead to very special band structures corresponding to chiral and wobbling phenomena. The chiral symmetry is expected for nuclei where total angular momentum have components along all the three mutually perpendicular axes with the collective rotor angular momentum directed along the medium axis, which has the largest moment of inertia within the irrotational model and $0 \leq \gamma \leq 60$. The angular momentum vectors of the valence particles align their angular momentum vectors along the short and long axis for particle- and hole-orbits, respectively. This arrangement of the three mutually perpendicular angular momentum vectors form two coordinate systems with opposite chirality, namely, with left and right handedness, corresponding to the left and right hand orientations of the three vectors. The operator transforming these two systems known as chiral operator ($\hat{\chi} = \hat{\mathcal{T}}\hat{\mathcal{R}}(\pi)$), first performs a rotation through 180° and then the time reversal operation, changing the directions of the angular momenta. The spontaneous breaking of chiral symmetry occurs in the intrinsic or body-fixed reference frame and in the laboratory frame with the restoration of this broken symmetry, it manifests in the appearance of chiral doublet bands, i.e., a pair $\Delta I = 1\hbar$ bands with the same parity.

Another observation that is only possible for triaxial systems is the wobbling motion and occurs when the rotation about the intermediate or medium axis having largest moment of inertia precesses about the fixed angular momentum vector because of the perturbations from the rotation of short and long axis. The wobbling motion, the classical analog of which is the spinning motion of an asymmetric top [16], is an excitation mode unique to a triaxial body. The rotation about the medium axis with the largest moment of inertia has the lowest energy and gives rise to the yrast states. The excited states near the yrast line are generated by transferring some angular momentum from the m -axis to s - and l -axes. It was shown by Bohr and Mottelson that for large angular momentum $I \gg 1$, a family of rotational bands are obtained which are characterized by the wobbling quantum number (n_ω). Considering the D_2 symmetry, one obtains the selection rule : $(-1)^{n_\omega} = (-1)^I$ [2] for even-even systems. Therefore, the band structures with even n_ω ($n_\omega = 0, 2, 4, \dots$) contain only even-spin states, and with odd n_ω ($n_\omega = 1, 3, \dots$) have only odd-spin members. The key characteristic feature of the wobbling bands is that the interband $I \rightarrow (I-1)$ transitions are predominantly E2 as compared with the transitions between the two signatures in normal rotational bands which are predominantly M1.

The wobbling excitation mode was first identified in ^{163}Lu [3] and subsequently was observed in $^{161,165,167}\text{Lu}$ [17,4,5] and ^{165}Tm isotopes [18]. Recently, the wobbling mode has also been observed in other mass regions [7,11,12,13,14,15]. The purpose of the present work is to perform a systematic investigation of the wobbling band structures observed in odd-mass isotopes using the microscopic approach of the triaxial projected shell model (TPSM) [19]. This model is now well established to provide a unified description of the properties of deformed and transitional nuclei [20,21,22,23,24,25,26,27]. The TPSM approach has been employed to perform a systematic investigation of the chiral band structures observed in various mass regions of the periodic table [28]. In a more recent work, a systematic analysis has been carried out for the γ bands observed in deformed nuclei and it has been demonstrated that staggering of the energies and $B(E2)$ transition probabilities of the γ bands can provide important information on the nature of the collective motion in atomic nuclei [29].

The present chapter is organized in the following manner. In the next section, we provide some basic elements of the wobbling motion as discussed in the original work of Bohr and Mottelson for even-even systems, and generalized to odd-mass systems by Hamamoto [16] and Frauendorf and Dönau [30]. In section 12.3, a survey of experimental results on the wobbling motion is provided. In section 12.4, the microscopic TPSM approach used in the present work is briefly discussed. In section 12.5, the results of the TPSM are presented and discussed in light of the available experimental measurements. In section 12.6, the present investigation on wobbling mode is summarized with some future perspectives.

2 Basic concepts of wobbling mode

Bohr and Mottelson in 1975 showed that wobbling mode in atomic nuclei for large angular-momentum, $I \gg 1$, will give rise to a family of band structures characterized by the phonon quantum number [2]. The properties of the wobbling bands were obtained using the triaxial particle-rotor model (TPRM) and in the present section, we shall follow the original work of Bohr and Mottelson [2].

Considering that the triaxial deformed field is time-reversal invariant, the leading order rotor Hamiltonian for an even-even system can be written as

$$\hat{H}_{rot} = \sum_{\kappa=1}^3 A_{\kappa} \hat{I}_{\kappa}^2 \quad , \quad (1)$$

where the coefficients A_{κ} are inverse of the moments of inertia (\mathcal{I}_{κ}) and are given by

$$A_{\kappa} = \frac{\hbar^2}{2\mathcal{I}_{\kappa}} \quad . \quad (2)$$

The axes are labeled such that $A_1 < A_2 < A_3$ or accordingly $\mathcal{I}_1 > \mathcal{I}_2 > \mathcal{I}_3$ and the yrast states have $|I_1| \sim I$.

The wobbling excitations are small amplitude oscillations of the angular momentum vector about the axis having the largest moment of inertia. The energy values are given by a harmonic spectrum of wobbling quanta [2]

$$E(n_\omega, I) = A_1 I(I+1) + (n_\omega + \frac{1}{2}) \hbar\omega, \quad (3)$$

where the quantum number n_ω gives the number of wobbling quanta and $\hbar\omega$ is the wobbling energy defined as the energy associated with wobbling excitation and is given by

$$\hbar\omega = 2I((A_2 - A_1)(A_3 - A_1))^{1/2} \quad (4)$$

The quadrupole transition probabilities are given by [2]

$$B(E2; n_\omega I \rightarrow n_\omega, I \pm 2) \approx \frac{5}{16\pi} e^2 Q_2^2 \quad (5)$$

$$B(E2; n_\omega I \rightarrow n_\omega - 1, I - 1) = \frac{5}{16\pi} e^2 \frac{n_\omega}{I} (\sqrt{3}Q_{0x} - \sqrt{2}Q_{2y})^2 \quad (6)$$

$$B(E2; n_\omega I \rightarrow n_\omega + 1, I - 1) = \frac{5}{16\pi} e^2 \left(\frac{n_\omega + 1}{I}\right) (\sqrt{3}Q_{0y} - \sqrt{2}Q_{2x})^2 \quad (7)$$

where, Q_0 and Q_2 are intrinsic quadrupole moments.

The excitations in wobbling mode are based on the quantum phonon model and have very special characteristics. In particular, the transitions from the $n_\omega = 2$ to the $n_\omega = 1$ should be a factor of two stronger as compared to the transitions from $n_\omega = 1$ to $n_\omega = 0$. On the other hand, the direct transition from $n_\omega = 2$ to $n_\omega = 0$ band are forbidden.

It was shown in the Refs. [16] and [30] that the presence of an odd-particle will modify the properties of wobbling motion in odd-mass systems. In particular, if the odd-particle occupies a low- K orbital of a high- j intruder orbital, the wobbling frequency will decrease [30] with angular-momentum, I and is referred to as the transverse wobbling (TW). This is in comparison to the longitudinal wobbling (LW), originally proposed by Bohr and Mottelson, for which the wobbling frequency increases with I . For odd-mass systems, the LW mode occurs if the odd-particle occupies a high- K orbital.

3 Survey of experimental data on wobbling mode

Although wobbling motion was originally predicted [2] for an even-even nucleus, but it was first experimentally established in the odd-proton nucleus ^{163}Lu [3]. For

this system, several triaxial strongly deformed (TSD) band structures were known to exist [31], however, the structure of these bands remained obscure as the transitions between the bands were not measured. In the seminal work [3], nine inter-connecting transitions were measured and it was possible to establish the structure of the two TSD bands, referred to as TSD1 and TSD2. It was demonstrated that these two bands have similar intrinsic structure with alignments (i_x) and moments of inertia ($J^{(2)}$) being almost identical. In the normal cranking picture [32], these bands are signature partner bands with TSD1 being the favoured partner having $\alpha = 1/2$ and TSD2 having $\alpha = -1/2$ with i_x of the later being different from the former as in the unfavoured branch, the aligned angular-momentum of the particle is tilted with respect to the rotational axis. In the case of the favoured signature band, the angular-momentum vector of the particle is aligned along the rotational axis. Further, in the cranking model the unfavoured signature band is expected at a higher excitation energy greater than 1 MeV and in the experimental data, its excitation energy relative to TSD1 band is less than 0.3 MeV. It has been shown using the particle-rotor model description that the observed features in ^{163}Lu could be explained by using three moments of inertia that correspond to the wobbling motion of a triaxial nucleus [33,34].

Electromagnetic properties provide a stringent test on the nature of the excitation mechanism observed in atomic nuclei [2]. In the cranking picture, $B(M1)$ transitions between $\alpha = -1/2$ and $+1/2$ signature partner bands are enhanced, whereas for the wobbling motion these $I \rightarrow (I-1)$ transitions are dominated by $B(E2)$. The angular-correlation, angular-distribution and polarization data [3] were found to be consistent with $M1/E2$ multipolarity for the connecting transitions with the mixing ratio (δ) of $(90.6 \pm 1.3)\%$ for the $E2$ and $(9.4 \pm 1.3)\%$ for the $M1$ transition. It was also noted that the phase of the zigzag pattern observed for $B(E2)_{out}/B(E2)_{in}$ and $B(M1)_{out}/B(E2)_{in}$ was opposite to that calculated in the cranking model and was consistent with the phase obtained for the wobbling mode in particle-rotor model calculations [3]. Moreover, in the quantal phonon model of the wobbling mode, which is valid for $I \gg 1\hbar$, the inter-band transitions follow special features with $B(E2)$ of the inter-band $I \rightarrow (I-1)$ transitions competing with those of the in-band $I \rightarrow (I-2)$ transitions. Further, the inter-band $B(E2)$ strength from the $n_\omega = 2$ to the $n_\omega = 1$ band should be a factor of two larger than the $B(E2)$ strength from the $n_\omega = 1$ to the $n_\omega = 0$ band [2,33,34]. These expected properties of the phonon wobbling mode have been experimentally verified for ^{163}Lu [35].

Candidate wobbling bands have also been reported in other neighbouring odd-A lutetium isotopes of $^{161,165,167}\text{Lu}$ [4,5,6,7], although the angular correlation and linear polarization measurements were not possible to confirm the $B(E2)$ character of the inter-band transitions as has been done for the ^{163}Lu isotope. Nevertheless, the similarity of the decay pattern of the TSD band structures of the three Lu isotopes with ^{163}Lu and large values obtained for the $B(E2)_{out}/B(E2)_{in}$ transitions, the structures have been designated as wobbling bands. The search for wobbling in other nuclides in this mass region failed to establish any more candidates, ex-

cept for ^{167}Ta [18]. It was demonstrated using the tilted axis cranking approach that the density of states for Lu isotopes is quite low for the TSD minimum and the wobbling bands could be identified. In other neighbouring nuclides, the density of states is quite high and particle-hole excitation modes are more favourable [36]. For ^{167}Ta , the similarity of the linking transitions between the TSD2 and TSD1 bands with the corresponding transitions in $^{163,165,167}\text{Lu}$ isotopes, the two TSD bands observed have been grouped as wobbling structures [18]. We would like to mention that TSD1 band in ^{167}Ta depicts a bandcrossing feature with $J^{(2)}$ showing a peak at about $\hbar\omega = 0.35$ MeV. This bandcrossing feature is also observed in ^{167}Lu , but not in other Lu isotopes.

In all the above systems, the wobbling bands have been established for the TSD minimum configuration with axial deformation value of ~ 0.40 . The wobbling mode for a normal deformed nuclide was reported for the first time in ^{135}Pr with $\varepsilon \sim 0.16$ [12]. Wobbling and signature partner (SP) band structures were delineated from the analysis of the angular distribution and polarization data. The mixing ratios determined from these measurements show large $B(E2)$ mixing for the transitions from $n_\omega = 1$ wobbling band to the yrast structure and for the SP band it is dominated by $B(M1)$. The evidence for the existence of a two-phonon wobbling band was provided in a subsequent work [13]. It needs to be added that new measurements have been performed and from the analysis of this new data, it has been shown that mixing ratio, $|\delta| < 1$, contradicting the wobbling interpretation of the observed bands in ^{135}Pr [37].

It was predicted [30] using the particle-rotor model that for the LW wobbling mode, the wobbling frequency initially will increase upto some critical angular-momentum and then will begin decreasing. However, in all the TW cases identified before 2020, wobbling frequency decreased with spin. It was shown in 2020 [38] that for one of the two TW wobbling bands identified in ^{183}Au , the frequency decreases initially and then after some spin values it increases. For the heavier ^{187}Au , a pair of longitudinal wobbling structures have been observed with the SP band [39].

The appearance of wobbling bands have also been reported in ^{127}Xe and ^{133}La through angular distributions and linear polarization measurements. The bands observed have been classified as $n_\omega = 0, 1, 2$ and SP bands [11,40]. In both these nuclei, the wobbling frequency decreases with spin and, therefore, has transverse character with angular-momentum of the particle along the s -axis. In ^{133}Ba , longitudinal wobbling mode has been proposed as for ^{135}Pr with wobbling frequency decreasing as a function of spin [41].

4 Triaxial projected shell model approach

Triaxial projected shell model approach is conceptually similar to the spherical shell model (SSM) and differing only in the way the basis space is chosen. TPSM employs the deformed intrinsic states of the triaxial Nilsson potential, which incorporate essential long-range correlations, as the basis configuration [42]. The truncation of the many-body basis in TPSM is very efficient as not only the numerical effort is drastically reduced, but also makes physical interpretation more transparent. The recently generalized TPSM approach with the inclusion of higher-order quasiparticle states has emerged as a powerful tool for exploring the triaxial characteristics of atomic nuclei as computational resources involved are quite modest and it is feasible to systematically investigate a broad range of atomic nuclei. As a matter of fact, several systematic investigations have been performed for chiral and γ vibrational band structures observed in triaxial nuclei [20,21,22,23,24,25,26,27]. The model space in the TPSM approach is spanned by multiquasiparticle basis states from different oscillator shells [43,44]. This allows to investigate high-spin band structures in well-deformed and transitional nuclei all across the nuclear chart.

The flow chart of the TPSM calculations can primarily be divided into three stages. In the first stage, the deformed basis are constructed by solving the triaxial Nilsson potential with a realistic set of quadrupole deformation parameters of ϵ and ϵ' for a given system under consideration. These deformation values lead to an accurate Fermi surface and it allows one to choose an optimum set of the basis states around the Fermi surface for a realistic description of the system. The standard Bardeen–Cooper–Schrieffer (BCS) procedure is then carried out to include the pairing correlations with the parameters given in Table 1.

The rotational symmetry is not conserved by the intrinsic states generated from the deformed Nilsson calculations and in the second stage this symmetry is restored through three - dimensional angular-momentum projection technique [45,46]. In this technique, good angular-momentum basis states are projected out from the Nilsson + BCS states using the explicit three- dimensional angular-momentum projection operator " P_{MK}^I " given by [47] :

$$\hat{P}_{MK}^I = \frac{2I+1}{8\pi^2} \int d\Omega D_{MK}^I(\Omega) \hat{R}(\Omega), \quad (8)$$

with the rotation operator

$$\hat{R}(\Omega) = e^{-i\alpha\hat{J}_z} e^{-i\beta\hat{J}_y} e^{-i\gamma\hat{J}_z}. \quad (9)$$

Here, " Ω " represents the set of Euler angles ($\alpha, \gamma = [0, 2\pi]$, $\beta = [0, \pi]$) and \hat{J}_s are the angular-momentum operators. The angular-momentum projection operator in Eq. (8) apart from projecting the good angular-momentum, also projects states with good K -values. The projected multi-quasiparticle basis states for different systems

are given for odd-proton nuclei as :

$$\begin{aligned} & \{ \hat{P}_{MK}^I a_{\pi_1}^\dagger |\Phi\rangle; \hat{P}_{MK}^I a_{\pi_1}^\dagger a_{v_1}^\dagger a_{v_2}^\dagger |\Phi\rangle; \hat{P}_{MK}^I a_{\pi_1}^\dagger a_{\pi_2}^\dagger a_{\pi_3}^\dagger |\Phi\rangle; \\ & \hat{P}_{MK}^I a_{\pi_1}^\dagger a_{\pi_2}^\dagger a_{\pi_3}^\dagger a_{v_1}^\dagger a_{v_2}^\dagger |\Phi\rangle \} \quad , \end{aligned} \quad (10)$$

and for odd-neutron nuclei :

$$\begin{aligned} & \{ \hat{P}_{MK}^I a_{v_1}^\dagger |\Phi\rangle; \hat{P}_{MK}^I a_{v_1}^\dagger a_{\pi_1}^\dagger a_{\pi_2}^\dagger |\Phi\rangle; \hat{P}_{MK}^I a_{v_1}^\dagger a_{v_2}^\dagger a_{v_3}^\dagger |\Phi\rangle; \\ & \hat{P}_{MK}^I a_{v_1}^\dagger a_{v_2}^\dagger a_{v_3}^\dagger a_{\pi_1}^\dagger a_{\pi_2}^\dagger |\Phi\rangle \} \quad , \end{aligned} \quad (11)$$

where $|\Phi\rangle$ in above equations represent the triaxial quasiparticle vacuum state and $a_{v_i}^\dagger, a_{\pi_i}^\dagger$ are quasiparticle creation operators, with the index $v_i(\pi_i)$, denoting the neutron (proton) quantum numbers and running over the selected single-quasiparticle states.

In the third and final stage, projected basis states given by Eqns. (10) and (11) are then used to diagonalize the shell model Hamiltonian. A two-body Hamiltonian in terms of separable forces is adopted which consists of the modified harmonic oscillator single-particle Hamiltonian and a residual two-body interaction comprising of quadrupole-quadrupole, monopole pairing and quadrupole pairing terms. These terms represent specific correlations which are considered to be essential to describe the low-energy nuclear phenomena [48]. The Hamiltonian has the following form :

$$\hat{H} = \hat{H}_0 - \frac{1}{2}\chi \sum_{\mu} \hat{Q}_{\mu}^{\dagger} \hat{Q}_{\mu} - G_M \hat{P}^{\dagger} \hat{P} - G_Q \sum_{\mu} \hat{P}_{\mu}^{\dagger} \hat{P}_{\mu}. \quad (12)$$

In the above equation, \hat{H}_0 is the spherical single - particle Hamiltonian containing the proper spin-orbit force for correct shell closures [49]. The QQ-force strength, χ , in Eq. (12) is related to the quadrupole deformation ε as a result of the self-consistent Hartree-Fock-Bogoliubov condition and the relation is given by [42]:

$$\chi_{\tau\tau'} = \frac{\frac{2}{3}\varepsilon\hbar\omega_{\tau}\hbar\omega_{\tau'}}{\hbar\omega_n \langle \hat{Q}_0 \rangle_n + \hbar\omega_p \langle \hat{Q}_0 \rangle_p}, \quad (13)$$

where $\omega_{\tau} = \omega_0 a_{\tau}$, with $\hbar\omega_0 = 41.4678A^{-\frac{1}{3}}$ MeV, and the isospin-dependence factor a_{τ} is defined as

$$a_{\tau} = \left[1 \pm \frac{N-Z}{A} \right]^{\frac{1}{3}},$$

with + (−) for $\tau =$ neutron (proton). The harmonic oscillation parameter is given by $b_{\tau}^2 = b_0^2/a_{\tau}$ with $b_0^2 = \hbar/(m\omega_0) = A^{\frac{1}{3}}$ fm². The monopole pairing strength G_M (in MeV) is of the standard form

$$G_M = \frac{G_1 \mp G_2 \frac{N-Z}{A}}{A}, \quad (14)$$

where the minus (plus) sign applies to neutrons (protons). The values of G_1 and G_2 are chosen such that the calculated gap parameters reproduce the experimental mass differences. The quadrupole pairing strength G_Q is assumed to be proportional to G_M , the proportionality constant being fixed as usual to be 0.16. The single-particle space for the TPSM usually includes three major harmonic oscillator shells (N) each for neutrons and protons in a calculation for deformed heavy nuclei. This large size of single-particle space accommodates sufficiently large number of active nucleons as well as all the important orbits and ensures the microscopic description of the collective motion. For different mass regions the oscillator shells employed are: N = 4, 5, 6 for neutrons and N = 3, 4, 5, for protons for A = 160 and 180 region; N = 3, 4, 5 for neutrons and N = 3, 4, 5, for protons for A = 130 region; N = 3, 4, 5 for neutrons and N = 2, 3, 4 for protons for A = 100 and 110 regions. The shell model Hamiltonian, Eq. (12) is diagonalized in the angular-momentum projected basis states, Eqns. (10) and (11), by following the Hill-Wheeler prescription [42]. The generalized eigen-value equation is given by

$$\sum_{\kappa' K'} \{ \mathcal{H}_{\kappa K \kappa' K'}^I - E \mathcal{N}_{\kappa K \kappa' K'}^I \} f_{\kappa' K'}^{\sigma I} = 0, \quad (15)$$

where the Hamiltonian and norm kernels are given by

$$\begin{aligned} \mathcal{H}_{\kappa K \kappa' K'}^I &= \langle \Phi_{\kappa} | \hat{H}_{KK'}^I | \Phi_{\kappa'} \rangle, \\ \mathcal{N}_{\kappa K \kappa' K'}^I &= \langle \Phi_{\kappa} | \hat{P}_{KK'}^I | \Phi_{\kappa'} \rangle. \end{aligned}$$

The Hill-Wheeler wave function is given by

$$\psi_{IM}^{\sigma} = \sum_{\kappa, K} f_{\kappa K}^{\sigma I} \hat{P}_{MK}^I | \Phi_{\kappa} \rangle. \quad (16)$$

where $f_{\kappa K}^{\sigma I}$ are the variational coefficients and index “ κ ” designates the basis states of Eqns. (10) and (11). The wave-function is then used to evaluate the electromagnetic transition probabilities. The reduced electric transition probabilities $B(EL)$ from an initial state (σ_i, I_i) to a final state (σ_f, I_f) are given by [50]

$$B(EL, I_i \rightarrow I_f) = \frac{1}{2I_i + 1} | \langle \psi^{\sigma_f I_f} | \hat{Q}_L | \psi^{\sigma_i I_i} \rangle |^2, \quad (17)$$

and the reduced matrix element can be expressed as

$$\begin{aligned}
& \langle \psi^{\sigma_f I_f} | \hat{Q}_L | \psi^{\sigma_i I_i} \rangle \\
&= \sum_{\kappa_i, \kappa_f, K_i, K_f} f_{\kappa_i K_i}^{\sigma_i I_i} f_{\kappa_f K_f}^{\sigma_f I_f} \sum_{M_i, M_f, M} (-)^{I_f - M_f} \\
&\quad \times \begin{pmatrix} I_f & L & I_i \\ -M_f & M & M_i \end{pmatrix} \\
&\quad \times \langle \Phi | \hat{P}_{K_f M_f}^{I_f} \hat{Q}_{LM} \hat{P}_{K_i M_i}^{I_i} | \Phi \rangle \\
&= 2 \sum_{\kappa_i, \kappa_f, K_i, K_f} f_{\kappa_i K_i}^{\sigma_i I_i} f_{\kappa_f K_f}^{\sigma_f I_f} \\
&\quad \times \sum_{M', M''} (-)^{I_f - K_f} (2I_f + 1)^{-1} \begin{pmatrix} I_f & L & I_i \\ -K_f & M' & M'' \end{pmatrix} \\
&\quad \times \int d\Omega D_{M'' K_i}^{I_i}(\Omega) \langle \Phi_{\kappa_f} | \hat{O}_{LM'} \hat{R}(\Omega) | \Phi_{\kappa_i} \rangle
\end{aligned}$$

Table 1

The axial deformation parameter (ε) and triaxial deformation parameter ε' employed in the calculation for odd-A mass nuclei. The axial deformation ε is taken from Refs. [4,5,16,18,51,52]. The asterisk (*) on ε is the deformation value for the positive parity bands in the ^{183}Au nucleus.

	^{161}Lu	^{163}Lu	^{165}Lu	^{167}Lu	^{167}Ta	^{105}Pd	^{127}Xe	^{131}Cs	^{133}Ba	^{133}La	^{135}Pr	^{151}Eu	^{183}Au	^{185}Au	^{187}Au
ε	0.400	0.400	0.380	0.430	0.370	0.257	0.150	0.140	0.150	0.150	0.160	0.200	0.280	0.270*	0.220
ε'	0.110	0.100	0.110	0.110	0.100	0.110	0.100	0.100	0.100	0.110	0.100	0.100	0.110	0.100	0.110
γ	15^0	14^0	16^0	14^0	15^0	23^0	34^0	36^0	34^0	36^0	32^0	27^0	21^0	20^0	27^0

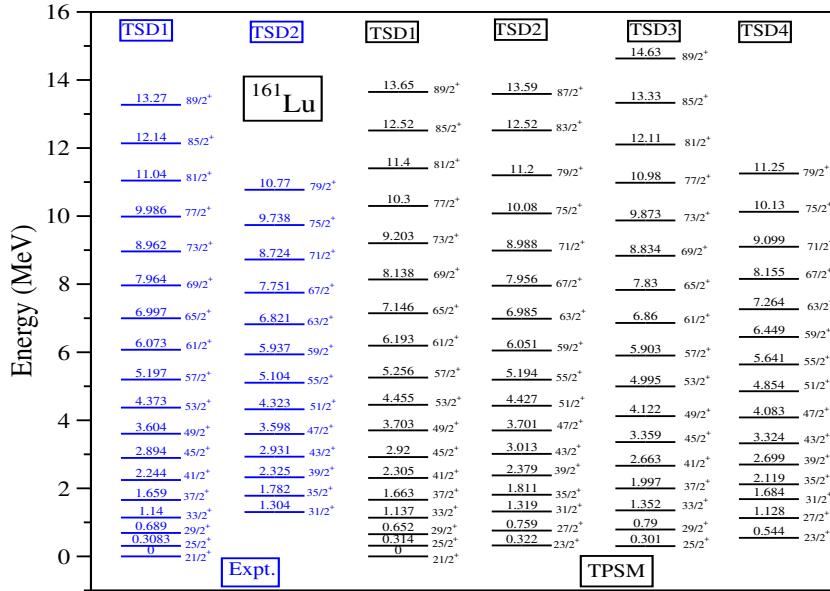


Figure 1. TPSM energies for the lowest four bands after configuration mixing are plotted along with the available experimental data for the ^{161}Lu isotope. Data is taken from [6].

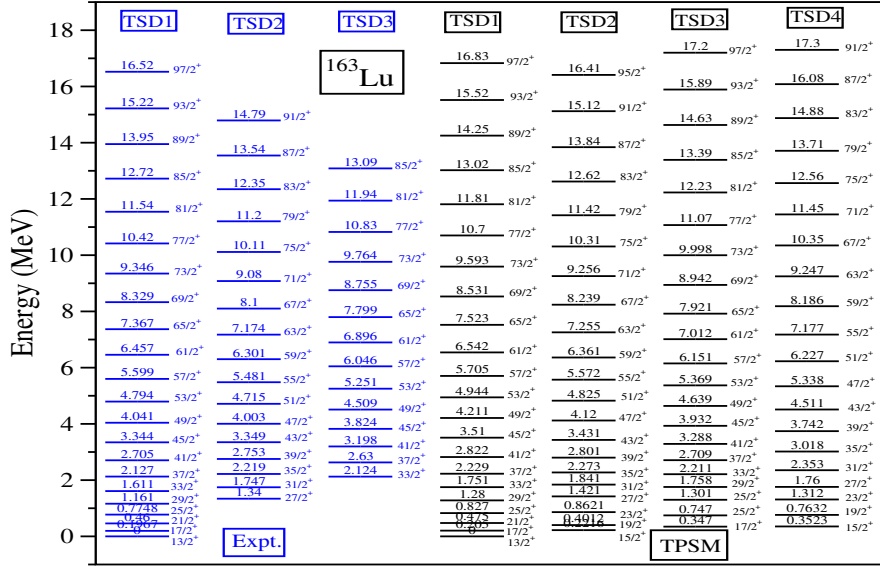


Figure 2. TPSM energies for the lowest four bands after configuration mixing are plotted along with the available experimental data for the ^{163}Lu isotope. Data is taken from [3].

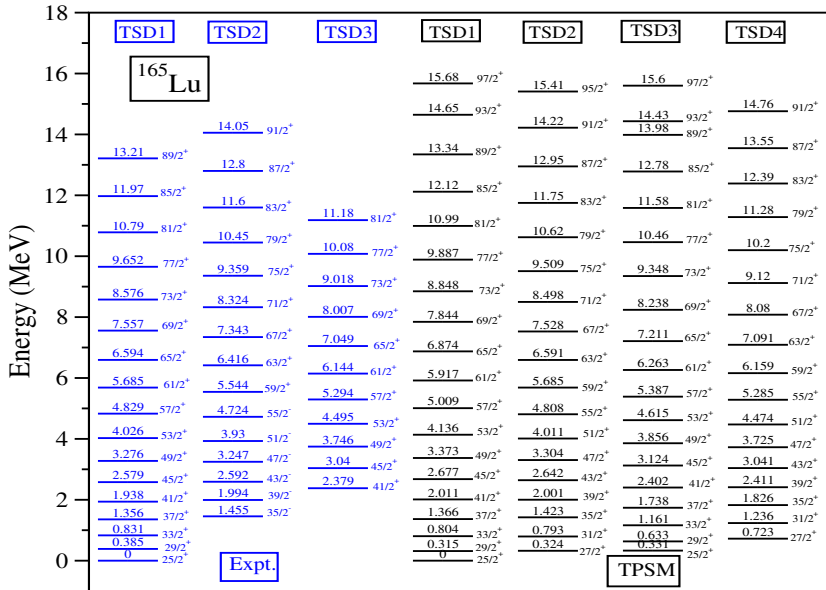


Figure 3. TPSM energies for the lowest four bands after configuration mixing are plotted along with the available experimental data for the ^{165}Lu isotope. Data is taken from [4].

5 Results and discussion

The TPSM calculations for $^{161,163,165,167}\text{Lu}$ and ^{167}Ta have been performed with the axial and non-axial deformation parameters given in Table 1. These quantities have been adopted from the earlier studies, in particular, from the ultimate cranking calculations [4,5,16,18,51] which predicted TSD shapes for these nuclei.

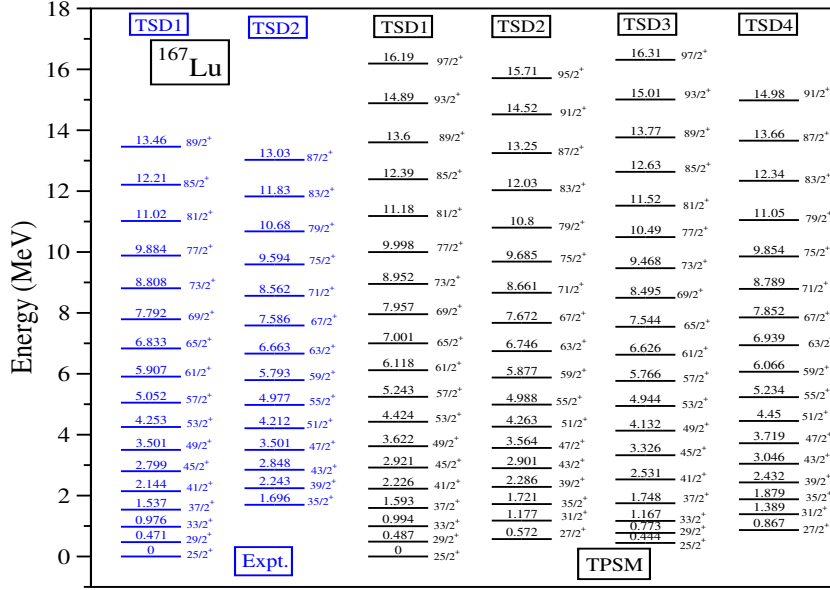


Figure 4. TPSM energies for the lowest four bands after configuration mixing are plotted along with the available experimental data for the ^{167}Lu isotope. Data is taken from [7].

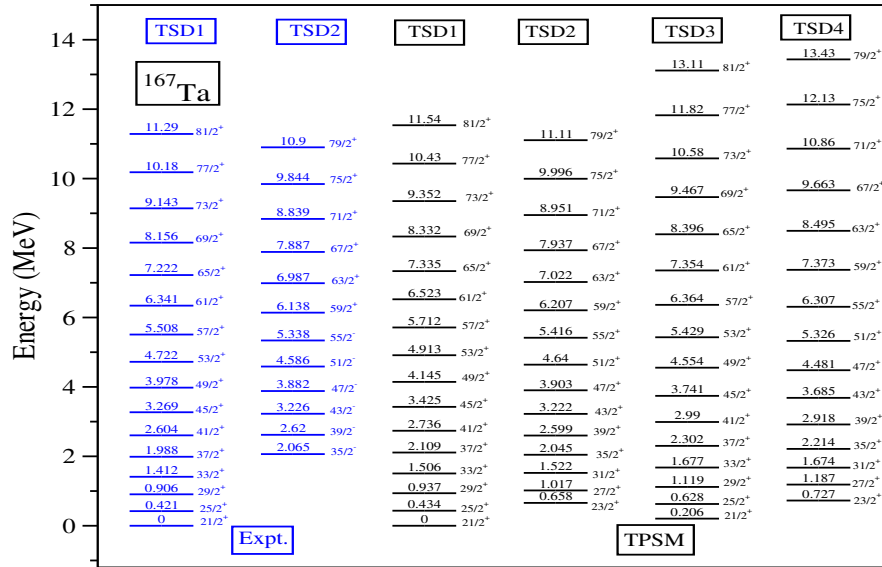


Figure 5. (Color online) TPSM energies for the lowest four bands after configuration mixing are plotted along with the available experimental data for the ^{167}Ta isotope. Data is taken from [18].

The TPSM energies obtained after diagonalization of the shell model Hamiltonian are compared with the available experimental data in Figs. 1, 2 3, 4 and 5. The calculated bands are depicted for the lowest two favoured ($\alpha = +1/2$) and two unfavoured ($\alpha = -1/2$) signature band structures. For ^{161}Lu , two TSD bands have been identified and are compared with the TPSM calculated band structures in Fig. 1. The experimental bands, labelled as TSD1 and TSD2, have been categorized as

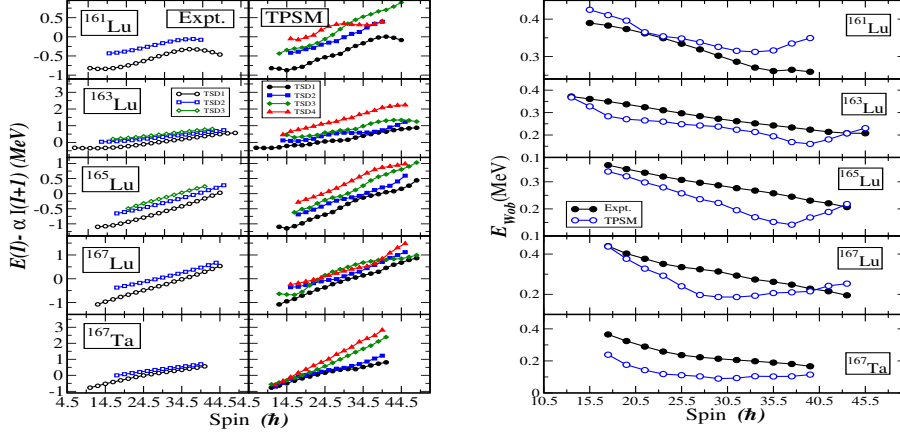


Figure 6. (Color online) (Left panel) TPSM energies for the lowest four bands after configuration mixing are plotted along with the available experimental data for $^{161,163,165,167}\text{Lu}$ and ^{167}Ta isotopes. The scaling factor $\alpha = 32.322A^{-5/3}$. (Right panel) TPSM wobbling energies are compared with the experimental values obtained from the bands TSD1 and TSD2 for $^{161-167}\text{Lu}$ and ^{167}Ta

$n_\omega = 0$ and 1 wobbling bands, based on the similarity of their properties with the corresponding band structures in ^{163}Lu . It is noted from Fig. 1 that TPSM energies for TSD1 and TSD2 bands are in good agreement with the experimental energies. The deviation of the TPSM energies is small at low-spin, but with increasing spin the difference is about 500 keV for the higher observed spin states. The TPSM energies for ^{163}Lu are compared with the experimental quantities in the Fig. 2 and it is again evident that TPSM approach reproduce the known energies quite well with a maximum deviation of about 550 keV at the highest spin, $I = 85/2$. For ^{163}Lu , three TSD bands have been identified and have been assigned as $n_\omega=0,1$ and 2. This is the first system where the occurrence of wobbling excitation mode was confirmed for the first time with the measurement of transition probabilities that will be discussed in detail later.

The calculated TPSM energies for ^{165}Lu and ^{167}Lu are compared with the experimental energies in Figs. 3 and 4. Three and two TSD bands have been identified for ^{165}Lu and ^{167}Lu , respectively and it is noted again that TPSM approach reproduces the data quite well. There are differences of about 300 keV for the highest angular momentum states in both the nuclei. The energies for ^{167}Ta are compared in Fig.5 for the two known TSD bands and it is noted that TPSM values are in reasonable agreement with the known energies.

To analyze the relative excitation energies of the wobbling bands, for the energies presented in Figs. 1, 2, 3, 4 and 5 a core contribution have been subtracted, and the resulting energies are presented in Figs. 6 (left panel). In the wobbling description, $n_\omega = 0$ TSD1 band is the result of the rotation of the system about the axis that has the largest moment of inertia, which is generally the m -axis. The excited $n_\omega = 1, 2$ and 3 wobbling bands are obtained when the angular-momentum from m -axis is

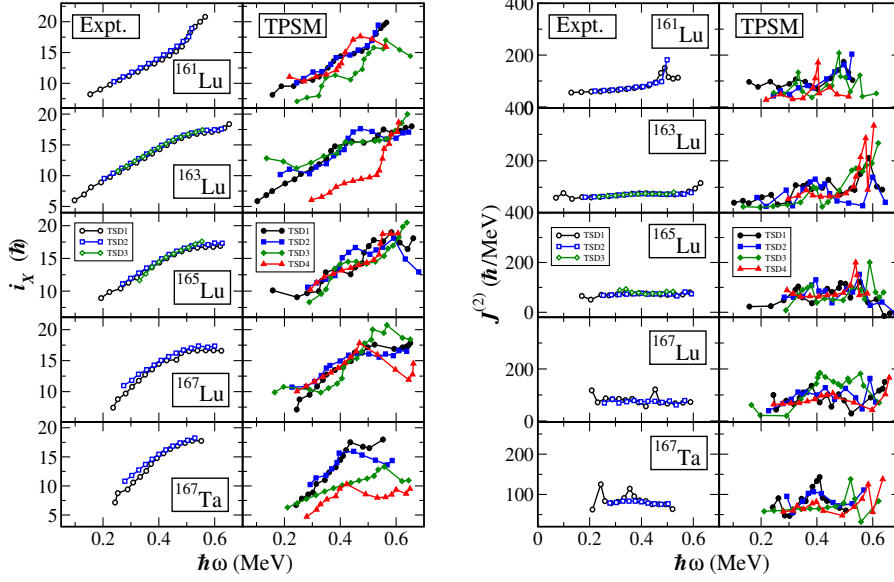


Figure 7. (Color online) (Left panel) Comparison of the aligned angular momentum, $i_x = I_x(\omega) - I_{x,ref}(\omega)$, where $\hbar\omega = \frac{E_\gamma}{I_x^I(\omega) - I_x^I(\omega)}$, $I_x(\omega) = \sqrt{I(I+1) - K^2}$ and $I_{x,ref}(\omega) = \omega(J_0 + \omega^2 J_1)$, obtained from the measured energy levels as well as those calculated from the TPSM results, for $^{161-167}\text{Lu}$ and ^{167}Ta nuclei. (Right Panel) Comparison between experimental and calculated dynamic moment of inertia, $\mathcal{J}^{(2)} = \frac{4}{E_\gamma(I) - E_\gamma(I-2)}$, for the TSD1, TSD2, TSD3 and TSD4 for $^{161-167}\text{Lu}$ and ^{167}Ta nuclei. The reference band Harris parameters used are $J_0=30$ and $J_1=40$ [4], obtained from the measured energy levels as well as those calculated from the TPSM results, for $^{161-167}\text{Lu}$ and ^{167}Ta nuclei.

transferred to l - and s -axis. The excitation energy of the first wobbling band is about 500 keV and the $n_\omega = 2$ band is less than 500 keV from the $n_\omega = 1$ band.

For the longitudinal motion, the rotational axis is along the long-axis and the wobbling frequency, defined as,

$$E_{wob}(I) = E_{n_\omega=1}(I) - [E_{n_\omega=0}(I+1) + E_{n_\omega=0}(I-1)]/2 \quad , \quad (18)$$

increases with spin [30]. For higher values of n_ω , the rotational axis moves away from the m -axis and will have smaller K -values along the m -axis. For the transverse wobbling motion, m -axis is replaced by s -axis and the wobbling frequency decreases with spin [30]. The wobbling frequency has been calculated from the excitation energies spectra and are displayed in Figs. 6 (right panel) for the studied Lu- and Ta nuclides. The calculated results are in good agreement with the experimental values and, in particular, the decreasing tendency of the wobbling energy as a function of angular momentum is reproduced in all the cases.

As the wobbling bands are based on the same intrinsic configuration, the aligned angular-momentum i_x and moments of inertia $J^{(2)}$ are expected to be identical. These quantities are depicted in Fig. 7 for the five nuclei. It is noted from the two

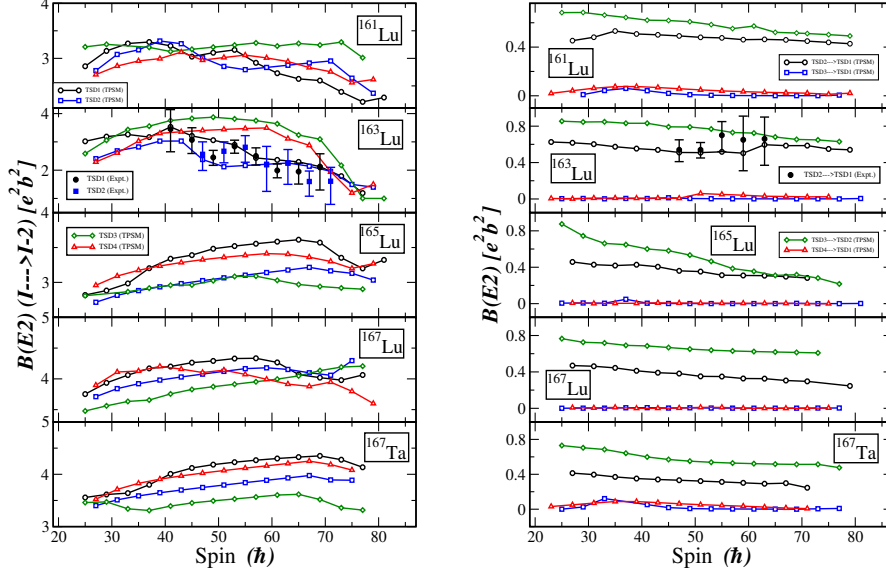


Figure 8. (Color online) Comparison between experimental and calculated $B(E2)_{in}$ (left panel) and $B(E2)_{out}$ (right panel) vs. spin for the TSD1, TSD2, TSD3 and TSD4 wobbling bands for $^{161-167}\text{Lu}$ and ^{167}Ta nuclei.

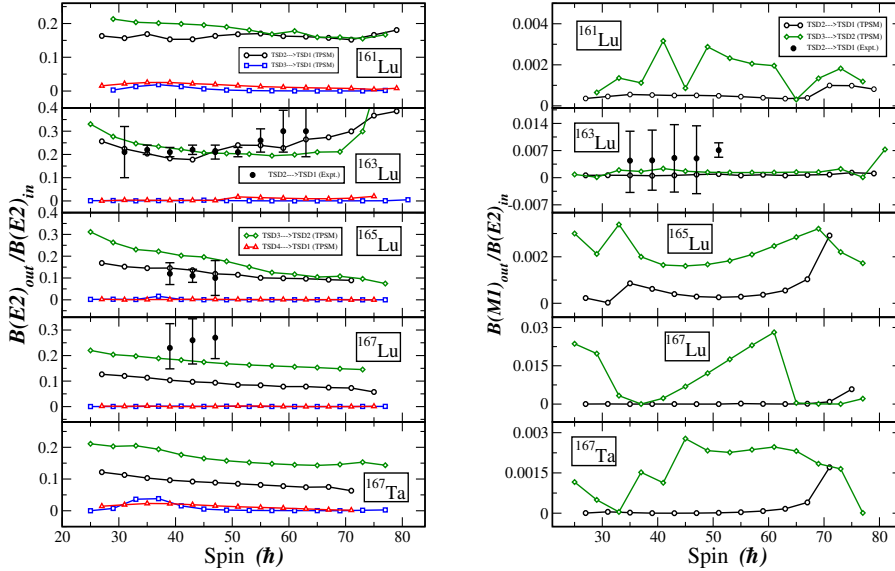


Figure 9. (Color online) Comparison between experimental and calculated $B(E2)_{out}/B(E2)_{in}$ (left panel) and $B(M1)_{out}/B(E2)_{in}$ (right panel) vs. spin for the TSD1, TSD2, TSD3 and TSD4 wobbling bands for $^{161-167}\text{Lu}$ and ^{167}Ta nuclei.

figures that i_x and $J^{(2)}$ obtained from the measured quantities are almost the same for all the wobbling bands. These quantities calculated using the TPSM values are also similar for the lowest two bands TSD1 and TSD2. However, the calculated quantities for the excited bands TSD3 and TSD4 are somewhat different in comparison to the lowest two bands.

The transition probabilities provide the important information on the nature of the excitation mechanism [2]. For the wobbling motion, the probabilities have the characteristic property that transitions from $n_\omega=1$ to $n_\omega=0$ are dominated by $B(E2)$ as compared to $B(M1)$ in the normal cranking picture for the transitions from the SP to the yrast band. Further, in the harmonic wobbling limit, the transitions from $n_\omega=2$ to $n_\omega=1$ are predicted to be a factor of two larger as compared to the transitions from $n_\omega=1$ to $n_\omega=0$, and direct transition from $n_\omega=2$ to $n_\omega=0$ are forbidden.

Before discussing the inter-band transitions, we first demonstrate the predictive power of the in-band $B(E2)$ transitions as these are measured to a good accuracy in some cases. These transitions are shown in Fig. 8 (left panel) for the lowest four bands of the five nuclei studied in the present work. The measured values are known for TSD1 and TSD2 bands of ^{163}Lu and the TPSM predicted values are noted to be in reasonable agreement with the known transitions. It is evident from the figure that for ^{161}Lu and ^{163}Lu , TSD1 and TSD2 in-band transitions are similar, however, for other bands these transitions vary for the four bands. It would be quite interesting to perform the experimental measurements of the the transition probabilities for other isotopes in order to confirm the varying nature of the predicted values.

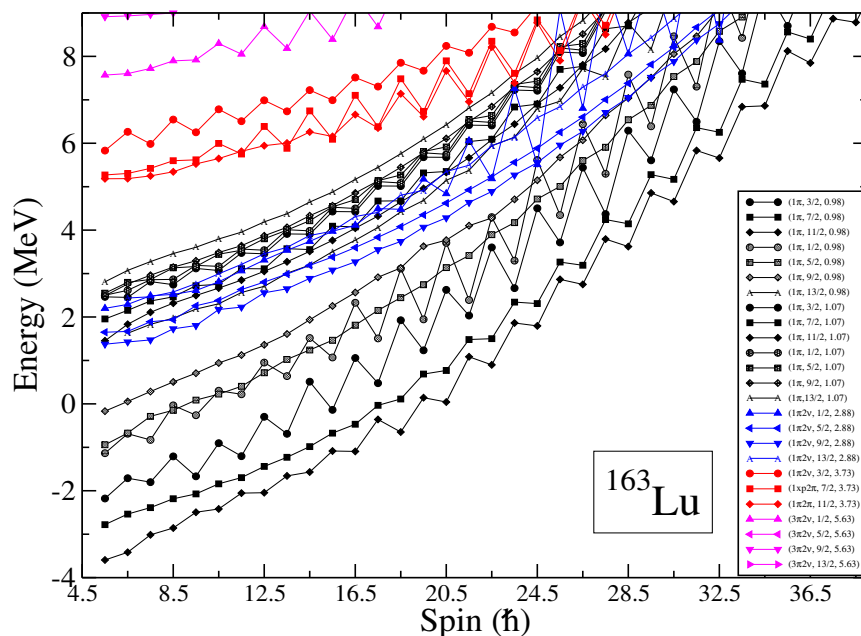


Figure 10. (Color online) Energies of the projected K -configurations with the short axis chosen as the quantization axis to which “ K ” quantum number refers. The curves are labelled by three quantities: quasiparticle character, K quantum number and energy of the quasiparticle state. For instance, $(1p, 3/2, 0.98)$ designates a one quasiproton state with $K = 3/2$ having intrinsic energy of 0.98 MeV.

The inter-band transitions among the four bands for the five isotopes are depicted in Fig. 8 (right panel). The $B(E2)$ transitions from TSD3 to TSD2 are clearly enhanced

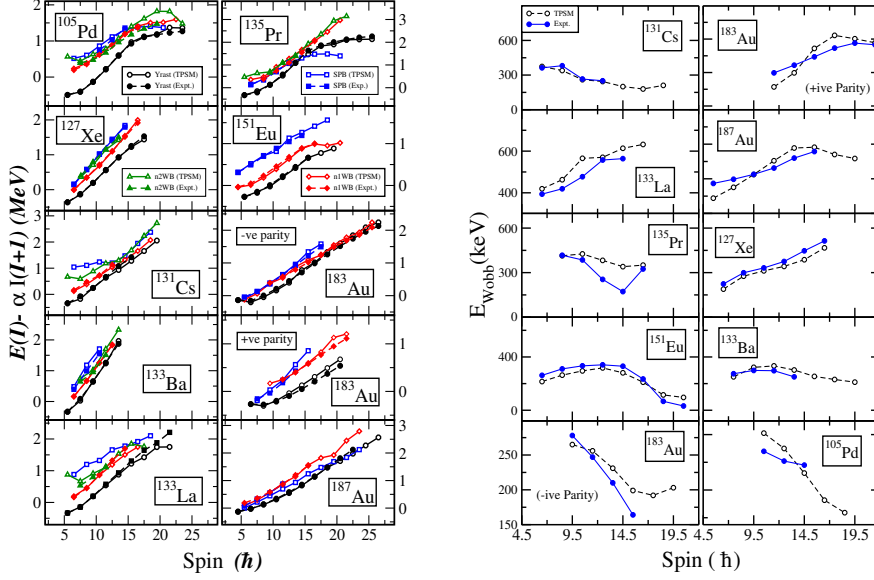


Figure 11. (Color online) (Left panel) TPSM energies for the lowest bands after configuration mixing are plotted along with the available experimental data for ^{105}Pd , ^{127}Xe , ^{131}Cs , ^{133}Ba , ^{133}La , ^{135}Pr , ^{151}Eu , ^{183}Au (-ve and +ve parity) and ^{187}Au nuclei. The scaling factor $\alpha = 32.322A^{-5/3}$. (Right panel) TPSM wobbling energies are compared with the experimental values obtained from the bands TW/LW for ^{105}Pd , ^{127}Xe , ^{131}Cs , ^{133}La , ^{133}Ba , ^{135}Pr , ^{151}Eu , ^{183}Au (negative parity), and ^{183}Au (positive parity). Data is taken from [11,12,13,14,15].

as compared to the transitions from TSD2 to TSD1 and direct transitions from TSD4 to TSD1, and TSD3 to TSD1 are retarded as expected for the harmonic wobbling mode. For ^{163}Lu , it is noted that TPSM predicted transitions for TSD2 to TSD1 are in good agreement with the measured transitions.

The TPSM calculated $B(E2)_{\text{out}}/B(E2)_{\text{in}}$ transition ratios are displayed in Fig. 9 (left panel) and are quite large as expected for the wobbling bands. The experimental ratios have been deduced from the DCO and polarization measurements for ^{163}Lu , ^{165}Lu and ^{167}Lu and are also displayed in Fig. 9. It is noted from the figure that for ^{163}Lu and ^{165}Lu , the TPSM values are in good agreement with the measured values, however, for ^{167}Lu the TPSM predicted values deviate for the three known data points. The $B(M1)_{\text{out}}/B(E2)_{\text{in}}$ ratios are plotted in Fig. 9 (right panel) and are seen to be quite small as compared to the $B(E2)_{\text{out}}/B(E2)_{\text{in}}$ ratios. These ratios have been measured for ^{163}Lu and TPSM calculated ratios are in good agreement.

To explore further that the above discussed wobbling bands are transverse in character, Fig. 10 depicts the energies of the bands projected from the quasiparticle configurations before the TPSM Hamiltonian is diagonalized for ^{163}Lu as an illustrative example. In the calculations, the short-axis is chosen as the quantization axis and “ K ” denotes the angular momentum projection on this axis. This is in contrast to the TPSM calculations published so far, where the long-axis is considered as the

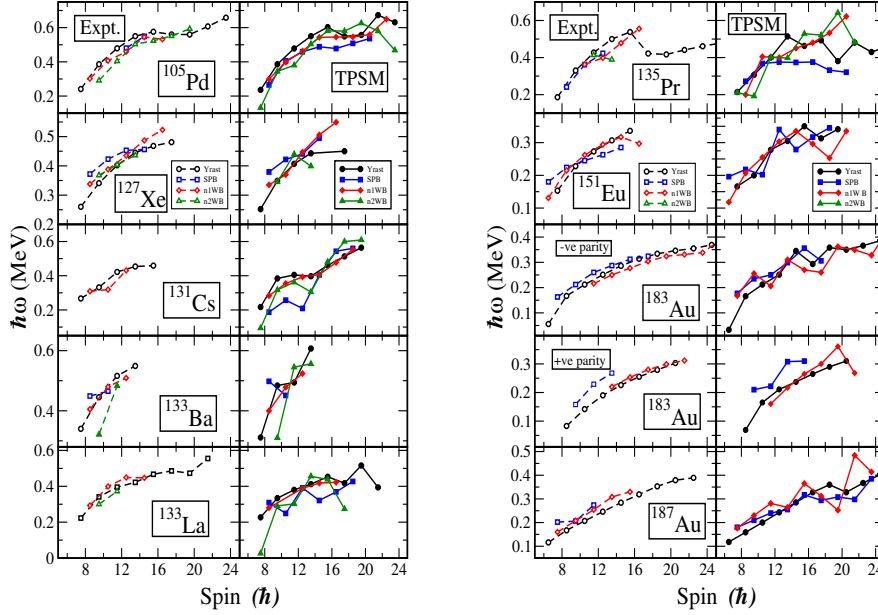


Figure 12. Experimental and calculated values from TPSM for the rotational frequency as functions of the spin I for the Bands $n_{\omega} = 0, 1$ and 2.

quantization axis. This choice simplifies the interpretation since in the TW regime, the odd quasiparticle tends to align its angular momentum along the short axis. Obviously, such a change of the quantization axis leaves the observables unchanged. Numerically, it is achieved by changing the triaxiality parameter γ to another equivalent sector that interchanges s - and l - axis. For this sector, the γ value is changed to the new value of $(-120^{\circ} - \gamma)$. It is noted from the figure that the yrast configuration corresponding to TSD1 ($\alpha = +1/2$) and TSD2 ($\alpha = -1/2$) band structures have $K=11/2$, which signifies that odd-proton is almost aligned towards the s -axis. The first excited band structures corresponding to TSD3 and TSD4 bands have $K=7/2$, indicating that for these band structures the rotational axis has moved away from the principle s -axis.

In the present work, we have also performed the TPSM calculations for ten wobbling bands observed in normal deformed nuclei with the deformation parameters employed listed in Table 1. On the left panel of Fig. 11, the excitation energies for the lowest bands for all the normal deformed wobbling cases are depicted against the known data and the behaviour of the wobbling frequency as a function of spin is also presented in Fig. 11 on the right panel. The frequency decreases for the cases of ^{131}Cs , ^{135}Pr , ^{151}Eu , ^{183}Au (negative parity), ^{133}Ba and ^{105}Pd , signifying that these nuclei have transverse wobbling mode. For ^{133}La , ^{187}Au (negative parity) and ^{127}Xe , the wobbling frequency increases with spin, which indicates that the collective motion has longitudinal character. For the positive parity wobbling band in ^{183}Au , the frequency first increases and then it decreases. It has been predicted for the TW motion that there is a critical spin up to which the frequency will increase and then after this spin value, the frequency will start decreasing [30]. It is noted

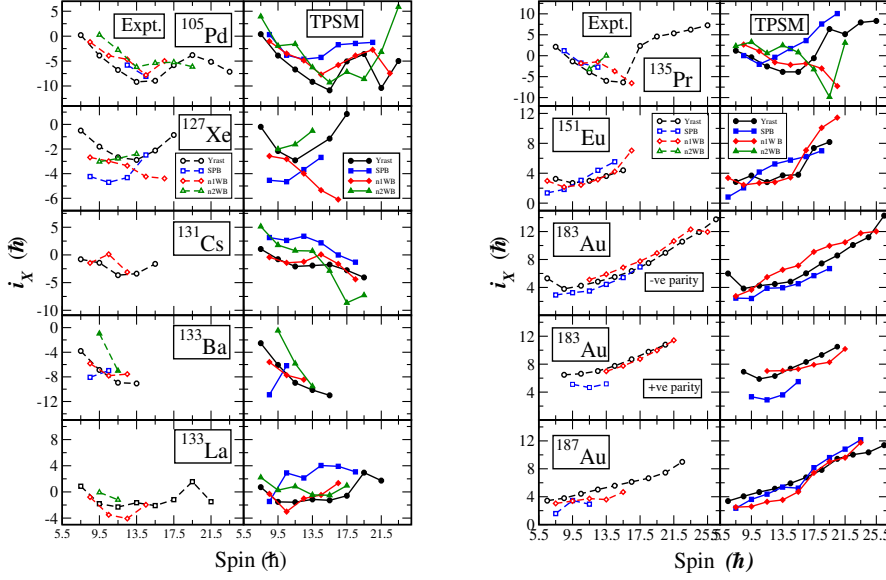


Figure 13. Comparison of the aligned angular momentum, $i_x = I_x(\omega) - I_{x,ref}(\omega)$, where $\hbar\omega = \frac{E_\gamma}{I_x(\omega) - I_x^f(\omega)}$, $I_x(\omega) = \sqrt{I(I+1) - K^2}$ and $I_{x,ref}(\omega) = \omega(J_0 + \omega^2 J_1)$, obtained from the measured energy levels as well as those calculated from the TPSM results, for ^{105}Pd , ^{127}Xe , ^{131}Cs , ^{133}La , ^{133}Ba , ^{135}Pr , ^{151}Eu , ^{183}Au (negative parity), and ^{183}Au (positive parity) nuclei. The reference band Harris parameters used are $J_0=16$ and $J_1=15$ [54].

that for the negative parity band in ^{183}Au , the TPSM predicts that the frequency will increase after $I=33/2$, and it would be interesting to verify this prediction in future experimental investigations. The derived rotational frequencies $\hbar\omega$ vs spin (I) are compared with the TPSM values in Fig. 12. The calculations reproduce the experimental data for all the ten wobbling bands observed in normal deformed nuclei.

To probe further the quasiparticle structures of the observed band structures, we have analyzed the alignments of the bands as a function of the spin and the results are presented in Fig. 13. The observed values are in the reasonable agreement with data. $B(E2)_{out}/B(E2)_{in}$ transitions for all the 10 nuclides are depicted in Fig. 14 (left panel). As already discussed, these transitions are crucial to establish the wobbling nature of the band structures. It is evident from the ratios that $B(E2)_{out}$ and $B(E2)_{in}$ have similar values which establishes the wobbling nature of these bands. On the other hand, the ratios $B(M1)_{out}/B(E2)_{in}$ displayed in Fig. 14 (right panel) are quite small as expected.

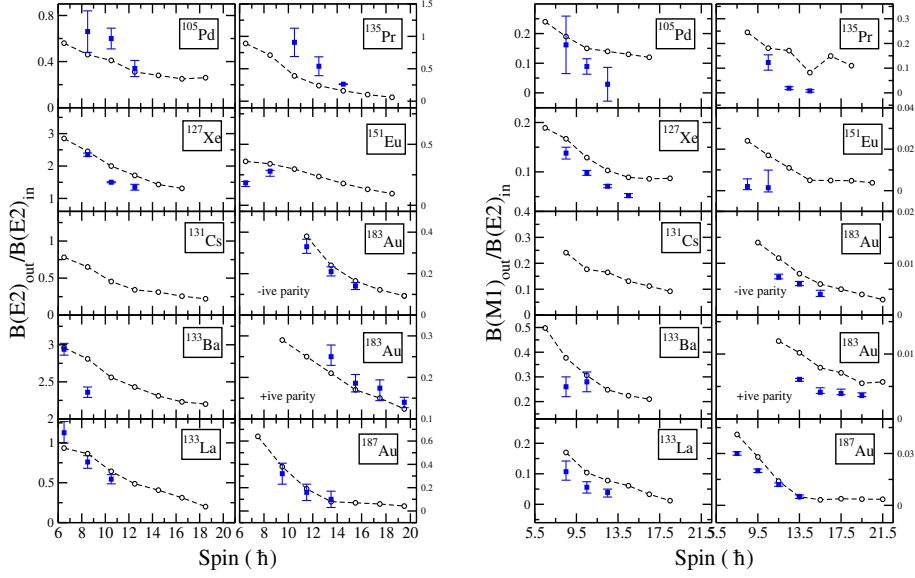


Figure 14. Comparison between experimental and calculated $B(E2)_{out}/B(E2)_{in}$ (left panel) and $B(M1)_{out}/B(E2)_{in}$ (right panel) vs. spin for the bands TW/LW for ^{131}Cs , ^{133}La , ^{135}Pr , ^{151}Eu , ^{183}Au (*negative* parity), ^{183}Au (*positive* parity), ^{127}Xe , ^{133}Ba and ^{105}Pd nuclei.

6 Summary and future perspectives

In the present work, we have performed a systematic investigation of the wobbling band structures observed in odd-mass nuclei. The analysis has been performed for fourteen nuclides using the triaxial projected shell model approach. This model is now well established as a method of choice to study the high-spin band structures in deformed and transitional nuclei. The TPSM approach employs the triaxial basis configurations and is well suited to investigate the properties of triaxial nuclei. It has been already used to perform a systematic study of the chiral band structures in atomic nuclei, which is a fingerprint of the triaxial deformation. The wobbling motion is another excitation mode which is only possible for triaxial shapes. This mode was originally predicted by Bohr and Mottelson [2] for an even-even system and it was shown that wobbling motion in the large I limit will give rise to a family of band structures, designated by the harmonic oscillator quantum number, n_ω . The characteristic feature of the wobbling mode is that transitions $I \rightarrow (I-1)$ from $n_\omega = 1$ to $n_\omega = 0$ bands are dominated by $B(E2)$ rather than $B(M1)$ as in the standard cranking model.

The wobbling mode was first identified in the odd-proton ^{163}Lu nucleus [3] and it was shown that the observed band structures obey all the characteristic features expected for the wobbling motion. Subsequently, the wobbling bands have also been observed in other nuclides and in the present work we have studied all these cases using the TPSM approach. It has been demonstrated that TPSM provides a reasonable description of the observed properties. In particular, the behaviour of

the wobbling frequency with spin is very well reproduced in all the studied cases. The in-band and inter-band transition probabilities have also been evaluated using the TPSM wavefunctions, and these have been shown to be consistent with the measured data.

In the normal TPSM analysis, long-axis is employed as the quantization axis. In order to analyse the results, we have used the short-axis as the quantization axis and is achieved by choosing the proper deformation values in another equivalent sector. This change of the axis simplifies the interpretation for cases where transverse wobbling is expected. For the TW motion, s -axis is the rotational axis and the resulting wavefunction will have large components along the s -axis. This has been shown for ^{163}Lu as an illustrative example of TW motion.

Further, the advantage of the TPSM approach is that it can describe the three dimensional wobbling mode and the standard cranking motion in a unified manner. In the normal cranking mode, SP bands are expected which have dominant $B(M1)$ transition probabilities, and we have demonstrated that the existence of wobbling and SP band structures identified in some nuclei can be simultaneously described using the TPSM approach. In the particle-rotor model picture, the wobbling and SP bands structures have very different geometry. For the case of excited wobbling bands, the rotational angular-momentum vector is tilted with respect to the principle axis and in the case of SP bands, it is the angular-momentum of the valence particle that is tilted and not the rotational axis. It is evident that the TPSM approach assimilates both these scenarios in a microscopic manner. In a more recent work [53], the TPSM approach has been used to substantiate the existence of a doublet wobbling excitation mode in ^{105}Pd .

In future, we intend to investigate the existence of wobbling motion in even-even systems. Several observed band structures in even-even nuclei have been proposed as candidate wobbling bands. These systems include, ^{130}Ba , ^{112}Ru , ^{134}Ce , ^{104}Pd , ^{114}Pd and $^{136,138}\text{Nd}$. In a few even-even systems, the odd-spin branch of the γ band is lower than the even-spin branch [30,55,56,57,58] in comparison to a large class of systems where it is opposite. These few nuclei have been categorized as γ rigid and it will be interesting to explore whether these systems have wobbling characteristics. The common feature is that the first excited band in these few nuclei is the odd-spin branch of the γ band and for the wobbling motion, it is also the odd-spin band having the harmonic oscillator quantum number, $n_{\omega}=1$.

7 Acknowledgement

The authors would like to acknowledge Nazira Nazir and S.P. Rouoof for their help in the preparation of some of the figures presented in the manuscript.

References

- [1] S. Frauendorf, *Int. J. Mod. Phys. E* **24**, 1541001 (2015).
- [2] A. Bohr and B. R. Mottelson, *Nuclear Structure*, Vol. II (Benjamin Inc., New York, 1975).
- [3] S. W. Ødegard, G. B. Hagemann, D. R. Jensen, M. Bergstrom, B. Herskind, G. Sletten, S. Tormanen, J. N. Wilson, P. O. Tjom, I. Hamamoto, K. Spohr, H. Hubel, A. Gorgen, G. Schonwasser, A. Bracco, S. Leoni, A. Maj, C. M. Petrache, P. Bednarczyk, and D. Curien, *Phys. Rev. Lett.* **86**, 5866 (2001).
- [4] G. Schönwaßer, H. Hübel, G. B Hagemann, P. Bednarczyk, G. Benzoni, A. Bracco, P. Bringel, R. Chapman, D. Curien, J. Domscheit, B. Herskind, D. R Jensen, S. Leoni, G. Lo Bianco, W. C. Ma, A. Maj, A. Neuser, S. W Odegard, C. M Petrache, D. Rosbach, H. Ryde, K. H. Spohr and A. K. Singh, *Phys. Lett. B* **552**, 9 (2003).
- [5] H. Amro, W. C. Ma, G. B. Hagemann, R. M. Diamond, J. Domscheit, P. Fallon, A. Gorgen, B. Herskind, H. Hubel, D. R. Jensen, Y. Li, A. O. Macchiavelli, D. Roux, G. Sletten, J. Thompson, D. Ward, I. Wiedenhover, J. N. Wilson and J. A. Winger, *Phys. Lett. B* **553**, 197 (2003).
- [6] P. Bringel, G. B. Hagemann, H. Hubel, A. Al-khatib, P. Bednarczyk, A. Burger, D. Curien, G. Gangopadhyay, B. Herskind, D. R. Jensen, D. T. Joss, Th. Kroll, G. Lo Bianco, S. Lunardi, W. C. Ma, N. Nenoff, A. Neuser-Neffgen, C. M. Petrache, G. Schonwasser, J. Simpson, A. K. Singh, N. Singh, and G. Sletten, *Eur. Phys. J. A* **24**, 167–172 (2005).
- [7] H. Amro, G. B. Hagemann, W. C. Ma, R. M. Diamond, J. Domscheit, P. Fallon, B. Herskind, H. Hubel, D. R. Jensen, Y. Li, A. O. Macchiavelli, D. Roux, G. Sletten, J. Thompson, I. Wiedenhover, J. N. Wilson, and J. A. Winger, *Phys. Rev. C* **71**, 011302 (2005).
- [8] S. Aberg, *Nucl. Phys. A* **520**, 35c (1990) and references therein.
- [9] I. Ragnarsson, *Phys. Rev. Lett.* **62**, 2084 (1989).
- [10] T. Bengtsson, *Nucl. Phys. A* **496**, 56 (1989); 512, 124 (1990).
- [11] S. Biswas, R. Palit, S. Frauendorf, U. Garg, W. Li, G. H. Bhat, J. A. Sheikh, J. Sethi, S. Saha, Purnima Singh, D. Choudhury, J. T. Matta, A. D. Ayangeakaa, W. A. Dar, V. Singh and S. Sihotra, *Eur. Phys. J. A* **55**, 159 (2019).
- [12] J. T. Matta, U. Garg, W. Li, S. Frauendorf, A. D. Ayangeakaa, D. Patel, K. W. Schlax, R. Palit, S. Saha, J. Sethi, T. Trivedi, S. S. Ghugre, R. Raut, A. K. Sinha, R. V. F. Janssens, S. Zhu, M. P. Carpenter, T. Lauritsen, D. Seweryniak, C. J. Chiara, F. G. Kondev, D. J. Hartle, C. M. Petrache, S. Mukhopadhyay, D. Vijaya Lakshmi, M. Kumar Raju, P. V. Madhusudhana Rao, S. K. Tandel, S. Ray and F. Donau, *Phys. Rev. Lett.* **114**, 082501 (2015).

- [13] N. Sensharma, U. Garg, S. Zhu, A. D. Ayangeakaa, S. Frauendorf, W. Li, G. H. Bhat, J. A. Sheikh, M. P. Carpenter, Q. B. Chen, J. L. Cozzi, S. S. Ghugre, Y. K. Gupta, D. J. Hartley, K. B. Howard, R. V. F. Janssens, F. G. Kondev, T. C. McMaken, R. Palit, J. Sethi, D. Seweryniak and R. P. Singh, *Phys. Lett. B* **792**, 170 (2019).
- [14] A. Mukherjee, S. Bhattacharya, T. Trivedi, S. Tiwari, R. P. Singh, S. Muralithar, Yashraj, K. Katre, R. Kumar, R. Palit, S. Chakraborty, S. Jehangir, Nazira Nazir, S. P. Rouoof, G. H. Bhat, J. A. Sheikh, N. Rather, R. Raut, S. S. Ghugre, S. Ali, S. Rajbanshi, S. Nag, S. S. Tiwary, A. Sharma, S. Kumar, S. Yadav, and A. K. Jain, *Phys. Rev. C* **107**, 054310 (2023).
- [15] J. Timár, Q. B. Chen, B. Kruzsicz, D. Sohler, I. Kuti, S. Q. Zhang, J. Meng, P. Joshi, R. Wadsworth, K. Starosta, A. Algora, P. Bednarczyk, D. Curien, Zs. Dombradi, G. Duchene, A. Gizon, J. Gizon, D. G. Jenkins, T. Koike, A. Krasznahorkay, J. Molnár, B. M. Nyaká, E. S. Paul, G. Rainovski, J. N. Scheurer, A. J. Simons, C. Vaman, and L. Zolnai, *Phys. Rev. Lett.* **122**, 062501 (2019).
- [16] I. Hamamoto, S. W. T0degård, G. B. Hagemann, D. R. Jensen, M. Bergstroem, B. Herskind, G. Sletten, S. Toermaenen, J. N. Wilson, P. O. Tjom, K. Spohr, H. Huebel, A. Goergen, G. Schoenwasser, A. Bracco, S. Leoni, A. Maj, C. M. Petrache, P. Bednarczyk, and D. Curien, *Acta Phys. Pol.* **B 32**, 2545 (2001).
- [17] P. Bringel, H. Hübel, A. Al-Khatib, A. Bürger, N. Nenoff, A. Neußer-Neffgen, G. Schönwasser, A. K. Singh, G. B. Hagemann, B. Herskind, D. R. Jensen, G. Sletten, P. Bednarczyk, D. Curien, D. T. Joss, J. Simpson, G. Gangopadhyay, Th. Kröll, G. Lo Bianco, C. M. Petrache, S. Lunardi, W. C. Ma, and N. Singh, *Phys. Rev. C* **73**, 054314 (2006).
- [18] D. J. Hartley, R. V. F. Janssens, L. L. Riedinger, M. A. Riley, A. Aguilar, M. P. Carpenter, C. J. Chiara, P. Chowdhury, I. G. Darby, U. Garg, Q. A. Ijaz, F. G. Kondev, S. Lakshmi, T. Lauritsen, A. Ludington, W. C. Ma, E. A. McCutchan, S. Mukhopadhyay, R. Pifer, E. P. Seyfried, I. Stefanescu, S. K. Tandel, U. Tandel, J. R. Vanhoy, X. Wang, S. Zhu, I. Hamamoto and S. Frauendorf, *Phys. Rev. C* **80**, 041304(R) (2009).
- [19] J. A. Sheikh and K. Hara, *Phys. Rev. Lett.* **82**, 3968 (1999).
- [20] G. H. Bhat, J. A. Sheikh, and R. Palit, *Phys. Lett. B* **707**, 250 (2012).
- [21] G. H. Bhat, W. A. Dar, J. A. Sheikh, and Y. Sun, *Phys. Rev. C* **89**, 014328 (2014).
- [22] S. Jehangir, G. H. Bhat, J. A. Sheikh, S. Frauendorf, S. N. T. Majola, P. A. Ganai, and J. F. Sharpey-Schafer, *Phys. Rev. C* **97**, 014310 (2018).
- [23] S. Jehangir, I. Maqbool, G. H. Bhat, J. A. Sheikh, R. Palit, and N. Rather, *Eur. Phys. J. A* **56**, 197 (2020).
- [24] S. Jehangir, G. H. Bhat, N. Rather, J. A. Sheikh, and R. Palit, *Phys. Rev. C* **104**, 044322 (2021).
- [25] S. Jehangir, G. H. Bhat, J. A. Sheikh, S. Frauendorf, W. Li, R. Palit, and N. Rather, *Eur. Phys. J. A* **57**, 308 (2021).

- [26] S. Jehangir, N. Nazir, G. H. Bhat, J. A. Sheikh, N. Rather, S. Chakraborty, and R. Palit, *Phys. Rev. C* **105**, 054310 (2022).
- [27] N. Nazir, S. Jehangir, S. P. Rouoof, G. H. Bhat, J. A. Sheikh, N. Rather, and S. Frauendorf, *Phys. Rev. C* **107**, L021303 (2023).
- [28] J. A. Sheikh, G. H. Bhat, W. A. Dar, S. Jehangir, and P. A. Ganai, *Phys. Scr.* **94**, 063015 (2016).
- [29] S. P. Rouoof, Nazira Nazir, S. Jehangir, G. H. Bhat, J. A. Sheikh, N. Rather, and S. Frauendorf, *Eur. Phys. J. A* **60**, 40 (2024).
- [30] S. Frauendorf and F. Dönau, *Phys. Rev. C* **89**, 014322 (2014).
- [31] H. Schnack-Petersen, R. Bengtsson, R.A. Bark, P. Bosetti, A. Brockstedt, H. Carlsson, L.P. Ekstrom, G.B. Hagemann, B. Herskind, F. Ingebretsen, H. J. Jensen, S. Leoni, A. Nordlund, H. Ryde, P. O. Tjom and C. X. Yang, *Nucl. Phys. A* **594**, 175 (1995).
- [32] S. Frauendorf, *Rev. Mod. Phys.* **73**, 463 (2001).
- [33] I. Hamamoto, *Phys. Rev. C* **65**, 044305 (2002).
- [34] I. Hamamoto and G. B. Hagemann, *Phys. Rev. C* **67**, 014319 (2003).
- [35] D. R. Jensen, G. B. Hagemann, I. Hamamoto, S. W. Odegård, B. Herskind, G. Sletten, J. N. Wilson, K. Spohr, H. Hubel, P. Bringel, A. Neuser, G. Schonwaser, A. K. Singh, W. C. Ma, H. Amro, A. Bracco, S. Leoni, G. Benzoni, A. Maj, C. M. Petrache, G. Lo Bianco, P. Bednarczyk, and D. Curien, *Phys. Rev. Lett.* **89**, 142503 (2002).
- [36] N. S. Pattabiraman, Y. Gu, S. Frauendorf, U. Garg, T. Li, B. K. Nayak, X. Wang, S. Zhu, S. S. Ghugre, R. V. F. Janssens, R. S. Chakravarthy, M. Whitehead, and A. O. Macchiavelli, *Phys. Lett. B* **647**, 243 (2007).
- [37] B. Lv and C. M. Petrache, *Symmetry* **15**, 1075 (2023).
- [38] S. Nandi, G. Mukherjee, Q. B. Chen, S. Frauendorf, R. Banik, Soumik Bhattacharya, Shabir Dar, S. Bhattacharyya, C. Bhattacharya, S. Chatterjee, S. Das, S. Samanta, R. Raut, S. S. Ghugre, S. Rajbanshi, Sajad Ali, H. Pai, Md. A. Asgar, S. Das Gupta, P. Chowdhury, and A. Goswami *Phys. Rev. Lett.* **125**, 132501 (2020).
- [39] N. Sensharma, U. Garg, Q. B. Chen, S. Frauendorf, D. P. Burdette, J.L. Cozzi, K.B. Howard, S. Zhu, M.P. Carpenter, P. Copp, F.G. Kondev, T. Lauritsen, J. Li, D. Seweryniak, J. Wu, A. D. Ayangeakaa, D. J. Hartley, R. V. F. Janssens, A. M. Forney, W. B. Walters, S. S. Ghugre, and R. Palit, *Phys. Rev. Lett.* **124**, 052501 (2020).
- [40] S. Chakraborty, H. P. Sharma, S. S. Tiwary, C. Majumder, A. K. Gupta, P. Banerjee, S. Ganguly, S. Rai, Pragati, Mayank, S. Kumar, A. Kumar, R. Palit, S. S. Bhattacharjee, R. P. Singh and S. Muralithar, *Phys. Lett. B* **811**, 135854 (2020).
- [41] K. Rojeeta Devi, Suresh Kumar, Naveen Kumar, Neelam, F. S. Babra, Md. S. R. Laskar, S. Biswas, S. Saha, P. Singh, S. Samanta, S. Das, S. Chakraborty, R. P. Singh, S. Muralithar and A. Kumar, *Phys. Lett. B* **823**, 136756 (2021).
- [42] K. Hara and Y. Sun, *Int. J. Mod. Phys. E* **04**, 637 (1995).

- [43] Nazira Nazir, S. Jehangir, S. P. Rouoof, G. H. Bhat, J. A. Sheikh, N. Rather, and Manzoor A. Malik, *Phys. Rev. C* **108**, 044308 (2023).
- [44] B. M. Musangu, E. H. Wang, J. H. Hamilton, S. Jehangir, G. H. Bhat, J. A. Sheikh, S. Frauendorf, C. J. Zachary, J. M. Eldridge, A. V. Ramayya, A. C. Dai, F. R. Xu, J. O. Rasmussen, Y. X. Luo, G. M. Ter-Akopian, Yu. Ts. Oganessian, and S. J. Zhu *Phys. Rev. C* **104**, 064318 (2021).
- [45] K. Hara and S. Iwasaki, *Nucl. Phys. A* **332**, 61 (1979)
- [46] K. Hara and S. Iwasaki, *Nucl. Phys. A* **348**, 200 (1980)
- [47] P. Ring and P. Schuck, *The Nuclear Many-Body Problem* (Springer-Verlag, New York), (1980).
- [48] K. Kumar and M. Baranger, *Nucl. Phys. A* **122**, 273 (1968).
- [49] S. G. Nilsson, C. F. Tsang, A. Sobiczewski, Z. Szymanski, S. Wycech, C. Gustafson, I. Lamm, P. Moller, and B. Nilsson, *Nucl. Phys. A* **131**, 1 (1969).
- [50] Y. Sun and J. L. Egido, *Nucl. Phys. A* **580**, 1 (1994).
- [51] R. Bengtsson and H. Ryde, *Eur. Phys. J A* **22**, 355 (2004).
- [52] P. Moller, J. R. Nix, W. D. Myers, and W. J. Swiatecki, *At. Data Nucl. Data Tables* **59**, 185 (1995).
- [53] A. Karmakar, P. Datta, N. Rather, G. H. Bhat, J. A. Sheikh, S. Jehangir, Q. B. Chen, S. Pal, R. Palit, A. Goswami, S. Chattopadhyay and S. Frauendorf, <https://doi.org/10.48550/arXiv.2403.08235> (2024).
- [54] C. M. Petrache, D. Bazzacco, S. Lunardi, C. Rossi Alvarez, G. de Angelis, M. De Poli, D. Bucurescu, C. A. Ur, P. B. Semmes, R. Wysset, *Nucl. Phys. A* **597**, 106-126 (1996).
- [55] Y. K. Wang, F. Q. Chen, and P. W. Zhao, *Phys. Lett. B* **802**, 135246 (2020).
- [56] J. Hamilton, S. Zhu, Y. Luo, A. Ramayya, S. Frauendorf, J. Rasmussen, J. Hwang, S. Liu, G. Ter-Akopian, A. Daniel, and Y. Oganessian, *Nucl. Phys. A* **834**, 28c-31c (2010).
- [57] C. M. Petrache, P. M. Walker, S. Guo, Q. B. Chen, S. Frauendorf, Y. X. Liu, R. A. Wyss, D. Mengoni, Y. H. Qiang, A. Astier, E. Dupont, R. Li, B. F. Lv, K. K. Zheng, D. Bazzacco, A. Boso, A. Goasduff, F. Recchia, D. Testov, F. Galtarossa, G. Jaworski, D. R. Napoli, S. Riccetto, M. Siciliano, J. J. Valiente-Dobon, M. L. Liu, X. H. Zhou, J. G. Wang, C. Andreoiu, F. H. Garcia, K. Ortner, K. Whitmore, T. Back, B. Cederwall, E. A. Lawrie, I. Kuti, D. Sohler, J. Timár, T. Marchlewski, J. Srebrny, A. Tucholski, *Phys. Lett. B* **795**, 241 (2019).
- [58] Q. B. Chen, S. Frauendorf, and C. M. Petrache, *Phys. Rev. C* **100**, 061301(R) (2019).